RESEARCH

Millimeter wave generation and uni-traveling carrier photodiode design based on its nonlinearity

Mingxi Yang[1] · Yongqing Huang[1] · Xuejie Wang[1] · Jihong Ye[1] · Shuhu Tan[1] · Xiaofeng Duan[1] · Kai Liu[1] · Xiaomin Ren[1]

Abstract

Nonlinear mechanism of photodetector in the communication band of 1550 nm was researched in this article. Then nonlinear frequency doubling mechanism was used to generate millimeter wave signals that can be used in millimeter wave communication systems. In the article, the layer structure of the photodetector was optimized to further improve the power of millimeter wave signals. Different from the fundamental frequency output power, the frequency doubling output signal exhibits completely different characteristics at low input optical power and high input optical power. Therefore, the structure design of the photodetector was optimized for different input optical power application scenarios. Finally, the influence of the incident optical field distribution on the nonlinear output of the photodetector was studied. The results showed that when the photodetector did not reach saturation, the Gaussian distribution situation could produce a larger nonlinear signal power than uniform distributed optical field.

1 Introduction

Millimeter wave communication, due to its characteristics of long wavelength and wide frequency band, can effectively solve many problems faced by high-speed wireless communication and therefore has a wide range of application prospects in communication systems. In the research of millimeter wave communication systems, the generation of millimeter wave signals has always been a research difficulty and hotspot. Conventionally, a microwave or mm-wave signal is generated using electronic circuitry with many stages of frequency doubling to achieve the desired frequency. The system is complicated and costly. In most application scenarios, the generated millimeter wave signals need to be transmitted to remote sites, and the high losses of transmission lines such as coaxial cables make the transmission of millimeter waves in the electrical domain impractical. Due to the high bandwidth and low loss characteristics of optical fibers, using optical fibers to transmit millimeter wave signals is an ideal solution. Therefore, using optical

methods to generate millimeter wave signals and then transmitting them to remote sites through optical fibers has become the main solution in millimeter wave communication systems [1].

In previous studies, many optical signal generation techniques have been proposed and proven to generate microwave or millimeter wave signals with low phase noise. These techniques can be divided into four categories: optical injection locking [2], optical phase-locked loop [3–9] (OPLL), millimeter wave generation using external modulation [10–13] and dual wavelength laser sources [14]. The above four technologies can effectively generate low phase noise millimeter wave signals, but their systems are relatively complex, and the output power is relatively low. Keith J. Williams et al. studied the generation and influencing factors of nonlinear signals in photodetectors in 1996 [15], providing theoretical support for the application of nonlinear signals in photodetectors. On this basis, in this article we utilize the nonlinear effects of photodetectors to generate output frequency doubling signals, with the frequency of the doubling signal selected in the category of millimeter waves. The method of generating millimeter wave signals based on the nonlinear mechanism of photodetectors is a technology in the field of microwave photonics, which effectively reduces the cost of the system. Besides, it can achieve the generation of frequency doubling signals while completing the photoelectric conversion steps, greatly

✉ Yongqing Huang
 yqhuang@bupt.edu.cn

1 State Key Laboratory of Information Photonics and Optical Communications, Beijing University of Posts and Telecommunications, Beijing, China

Table 1 Initial epitaxial layer structure

Layer	Material	Bandgap (eV)	Thickness (nm)	Dopant Type	Doping Level (cm^{-3})
P contact	InGaAs	0.73	50	P	3e19
Block	InGaAsP	1.105	20	P	2e19
P absorption	InGaAs	0.73	220	P	1e18
Gap grading	InGaAs	0.73	80	Undoped	1e15
Gap grading	InGaAsP	1.0	16	Undoped	1e15
Gap grading	InP	1.35	6	Undoped	1e15
Cliff	InP	1.35	7	N	1e18
Collection	InP	1.35	263	N	1e16
Sub Collection	InP	1.35	50	N	5e18
N contact	InP	1.35	500	N	1e19

simplifying the complexity of the system. To obtain higher millimeter wave signals power compared to other methods, this article simultaneously optimizes the layer structure and optical field distribution of photodetectors. This alleviated the bandwidth limitation of photodetectors on the system, and can be adapted to any system, which increasing the practicality of generating millimeter wave signals based on the nonlinear mechanism of photodetectors.

2 Photodetector structure

The millimeter wave frequency range usually refers to 30 GHz to 300 GHz, the selection of the initial structure of the photodetector is particularly important. Firstly, the photodetector needs to have sufficient bandwidth to generate millimeter wave signals. Taking a 30 GHz millimeter wave signal as an example, using frequency doubling to generate a 30 GHz signal requires the photodetector to have a working bandwidth of at least 15 GHz. Secondly, the saturation

power of the device should be as high as possible, as higher saturation power can enable the photodetector to operate at higher optical power, facilitating the generation of nonlinear signals. Therefore, for the selection of the initial structure, it needs to have a dual advantage of bandwidth and output power.

The structure of the photodetector used in the simulation section of this article is shown in Table 1 [16]. The device's absorption layer consists of a 220 nm P-type absorption layer and an 80 nm depletion absorption layer. In order to suppress the heterojunction barrier at the interface between the absorption layer and the collection layer during structural design, a step gradient bandgap was used and an InGaAsP layer was inserted between the InGaAs absorption layer and the InP collection layer. The device has a response of 0.2 A/W and a 3dB response bandwidth of 16 GHz in the active region with a diameter of 20 μm. In addition, the device structure is designed for high-power application scenarios, making it suitable for generating millimeter wave signals.

3 Nonlinear mechanisms and the generation of millimeter wave signals

The input and output of the photodetector have a non-linear correspondence. As shown in Fig. 1, when the input optical signal is a single frequency sine wave signal, there is a certain degree of distortion in the output current, which will introduce a new frequency component in frequency domain, which is an integer multiple of the fundamental frequency. Therefore, the nonlinear characteristics of photodetectors can be utilized to generate frequency doubling electrical signals.
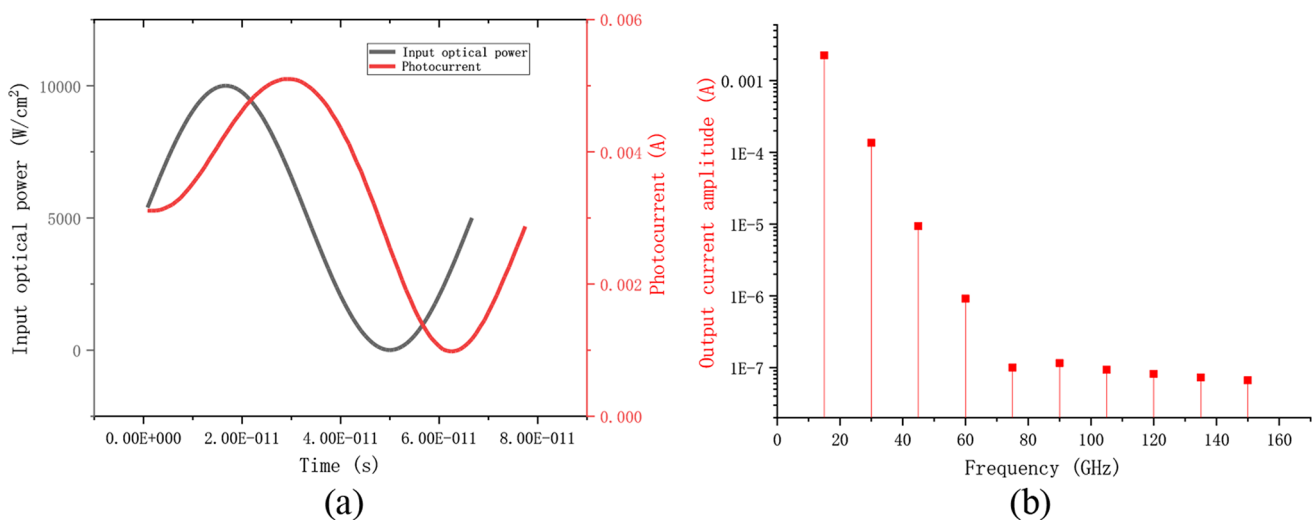

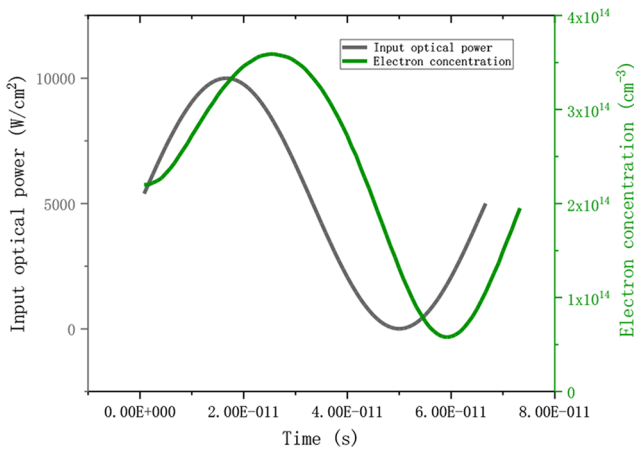**Fig. 1** Input and output waveforms of photodetector within one period(**a**) Spectrum diagram of output current(**b**)

Fig. 2 Electron concentration of the collection layer changes within one period

Fig. 3 The variation of DC output power, fundamental frequency power, and harmonic power of photodetectors with input optical power

For UTC-PD, changes in electron concentration can effectively reflect the spatial charge effect within the device. As the input optical power increases, photo-generated Carriers will gradually accumulate inside the device, generating an electric field opposite to the direction of the built-in electric field, causing a change in the intensity of the built-in electric field in the device, thereby affecting the carrier transition time inside the device and the output power of the device. This article extracts the variation of electron concentration at the center position of the photodetector collection layer (Fig. 2) within one period: Ideally, the electron concentration in the device collection layer should increase with the increase of input optical power and decrease with the decrease of input optical power, and their changes are synchronous. The variation curve of electron concentration in the figure shows significant distortion compared to the variation curve of input light power, which will cause the impact of space charge effect on the device to not match the waveform of the input signal. The electric intensity inside the photodetector does not change linearly, resulting in distortion of the output signal of the device, which is the reason for the generation of nonlinear signals.

Firstly, the frequency response of UTC-PD under large signal (modulation depth of 100%) input is obtained through Atlas device simulator of Silvaco TCAD, i.e. I(ω). Then, according to the report by G. Ghione et al. [17], the RF output power $P_{out}(\omega)$ of the device was calculated when considering the ideal load impedance $R_L=50\ \Omega$ and the effects of the coupling resistance (R_s), parasitic capacitance (C_p), and junction capacitance (C_J) The formula is as follows:

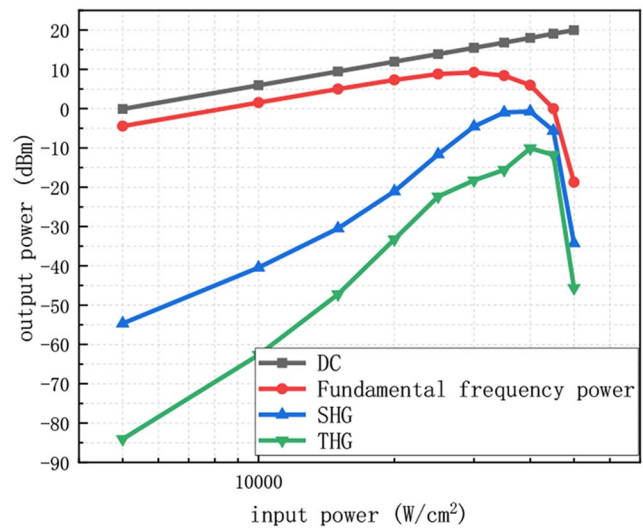$$P_{out}(\omega) = \left(\frac{I(\omega)}{\sqrt{1+\omega^2(R_S+R_L)^2(C_P+C_J)^2}}\right)^2 R_L \qquad (1)$$

Where $\omega=2\pi f$ is the angular frequency. The capacitance values of photodiodes under different conditions are calculated through C-V curve simulation. The simulation calculation takes into account the parasitic capacitance of 5fF caused by metal electrodes and the series resistance of 15 Ω [18]. Due to the consideration of factors such as series resistance, parasitic capacitance, external load impedance, and device structure in the physical model, it is reasonable to use this method to numerically solve the output power of UTC-PD. Although the above model does not take into account the impact of parasitic inductance on device performance, smaller inductance values are advantageous for device performance (parasitic inductance is usually smaller), and larger inductance needs to be led through special electrode design. Therefore, the RF output power value calculated by the above model is closer to the actual situation.

According to the above method, the DC output power (DC), fundamental power (Fundamental), second-order harmonic power (SHG), and third-order harmonic power (THG) of the photodetector were simulated and calculated as a function of the input optical power, as shown in Fig. 3. The simulation conditions were set as follows: the reverse bias of the device was 1 V, the active region diameter of the device was selected as 20 μm. The modulation frequency of the input optical signal is 15 GHz, the incident beam wavelength is 1550 nm. Under this working condition, a 30 GHz doubling frequency signal can be generated, which belongs to the frequency range of millimeter waves. As shown in the figure, the fundamental frequency signal reaches saturation at an input optical power of $3\times10^4 \mathrm{W/cm^2}$, and the saturation points of the second and third harmonic signals also appear near the fundamental frequency saturation point. The output doubling frequency signal reaches its maximum at

an input optical power of $3 \times 10^4 \mathrm{W/cm^2}$, with a maximum power of 0dBm.

Figure 4 shows the variation of the fundamental output power and second-order harmonic power of the photodetector with the input optical frequency. The fundamental power decreases with the increase of the input optical frequency, which is the normal frequency response curve of the device. Correspondingly, the second harmonic power also decreases with the increase of input optical frequency, And the slope of the curve is approximately twice of fundamental frequency power. The nonlinear mechanism of photodetectors can generate a second harmonic signal of any frequency. In order to ensure the amplitude of the generated signal and meet the requirements of millimeter wave communication systems, 15 GHz was selected in the article.

4 Structural design of photodetector

The nonlinear mechanism of photodetectors can generate frequency doubling signals for millimeter wave communication systems, but under initial structural conditions, the power of frequency doubling signals provided by photodetectors is very limited. According to the mechanism of nonlinear signal generation mentioned earlier, the essence of frequency doubling signal generation is caused by the space charge effect inside the photodetector. This article will optimize the layer structure of the photodetector to generate higher frequency doubling output power.

Simulation analysis (Fig. 5) shows the variation curves of the fundamental frequency (a) and second harmonic (b) power of the photodetector with input optical power under different biases: for the fundamental frequency power, the variation rules under different biases are consistent, and
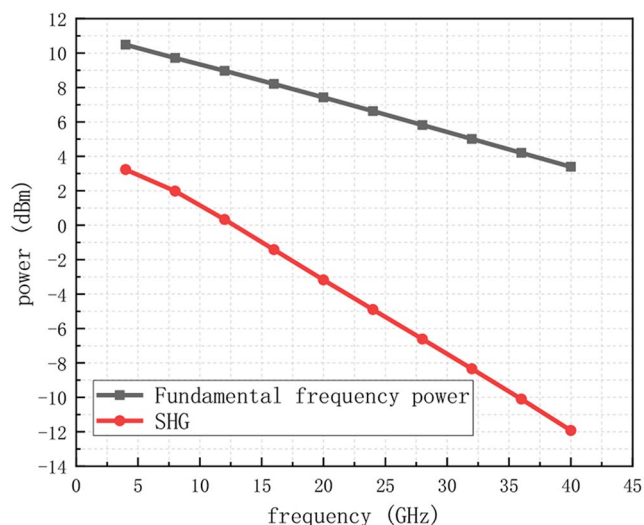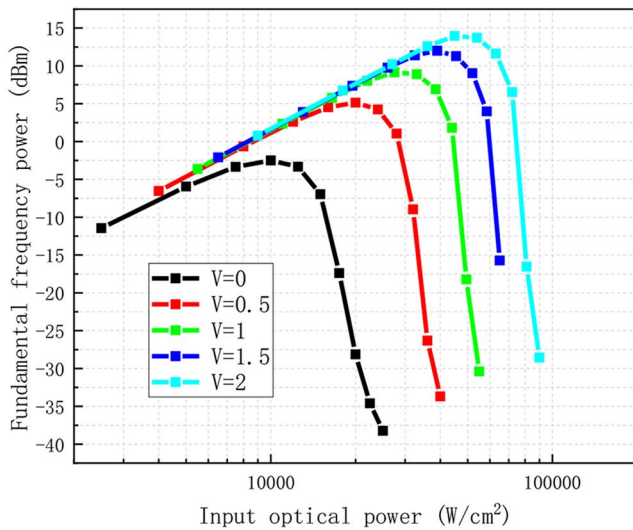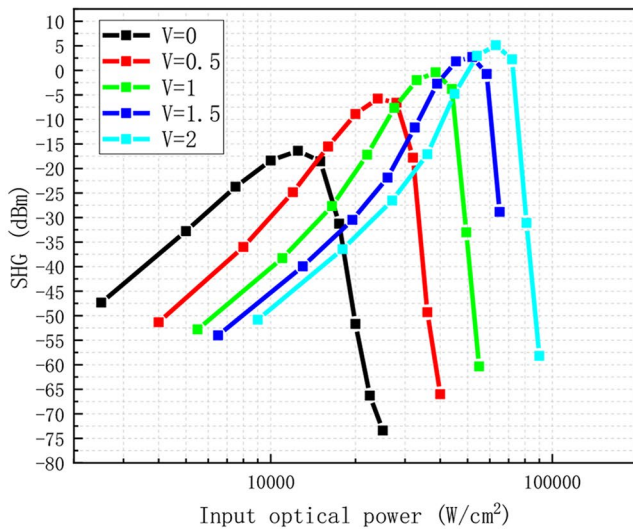

Fig. 4 The variation of fundamental frequency and second-order harmonic power of photodetectors with input optical frequency

they tend to saturate with the increase of optical power. After saturation point, the RF output power gradually decreases. Under different bias conditions, the fundamental output power at low bias is always lower than that at high bias. This is because under higher bias operating conditions, the internal electric field of the device is higher, which can effectively suppress the space charge effect. When the device is saturated, the input optical power is higher, and the corresponding fundamental output power is higher at the saturation point of the device. Unlike the variation trend of fundamental power, the output power of the second harmonic exhibits different characteristics when the input optical power is low and high: when the input optical power of the device is high (the input optical power reaches saturation point), the variation trend of the second harmonic power and fundamental power is consistent, both tending to saturation with the increase of optical power, and the output power of the second harmonic gradually decreases after saturation point. Under different bias conditions, the peak second harmonic output power at low bias is lower than that at high bias. When the input optical power of the device is low (the input optical power has not reached the saturation point), the second harmonic signal power actually decreases with the increase of bias voltage. The reason is that under low bias voltage, the internal electric field of the device is smaller, and the space charge effect of the device is stronger. The stronger space charge effect directly leads to a larger nonlinear signal power.

From this, it can be seen that the factors affecting the nonlinear signal power of the photodetector are essentially caused by the space charge effect: when the input optical power is low (the optical power has not reached the saturation point), the power of the nonlinear signal is determined by the space charge effect under working conditions. Reducing the bias voltage and increasing the input optical power can increase the power of the nonlinear signal by enhancing the space charge effect; When the input optical power is high (reaching the saturation point), the saturation effect caused by space charge effect affects the nonlinear signal power. When the photodetector reaches the AC saturation point, the fundamental frequency power and harmonic power of each order rapidly decrease. In this case, a higher internal electric field can better suppress the saturation phenomenon caused by space charge effect, and the device can reach saturation under larger input optical power conditions, The corresponding fundamental power and harmonic power of each order will also be higher. From this, it can be seen that optimizing the structure of photodetectors requires separate discussions on the high and low input optical power. For fixed or low input optical power, the device design should strive to enhance the space charge effect to obtain a larger frequency doubling signal; For larger or unrestricted input

(a)

(b)

Fig. 5 The variation of fundamental frequency power (**a**) and second harmonic power (**b**) of photodetectors under different bias voltages with input optical power

power, the device design should try to suppress the space charge effect as much as possible to achieve higher saturation power of the device, which will result in a larger frequency doubling signal.

Next, we will optimize the design of photodetectors for millimeter wave signal generation based on their high input optical power and low input optical power, respectively.

4.1 Low input optical power situation

This section we will optimize the device structure based on mentioned earlier. Firstly, the photodetector operating at a fixed or small input power will be optimized, with a diameter of 20 μm in the active region of the device. We will study
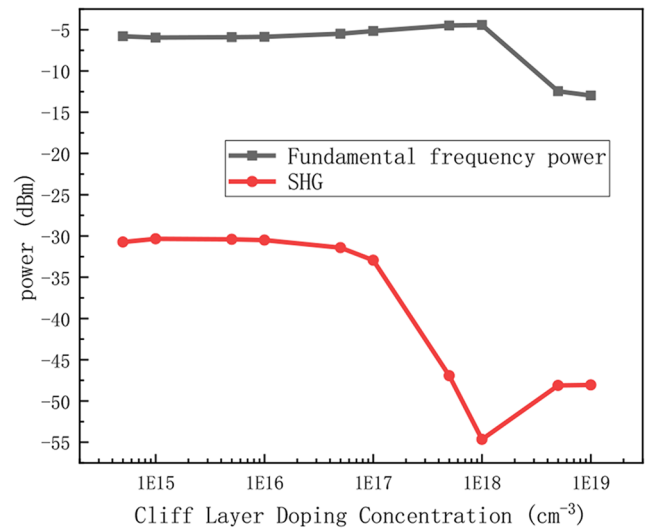

Fig. 6 The variation of fundamental frequency power and second harmonic power with cliff layer doping concentration (Low input optical power situation)

the amplitude of 30 GHz millimeter wave signals generated by devices with different structures under the conditions of a bias voltage of 1 V, the modulation frequency of the input optical signal is 15 GHz, and a peak incident optical power of 5×10^3 W/cm².

Figure 6 shows the variation of fundamental frequency output power and second harmonic power of the device with initial structure (The thickness of the collection layer is 263 nm) under different doping concentrations of cliff layers. The initial doping concentration point (5×10^{14}) in the figure represents the structure of the device without cliff layers. When the doping concentration of cliff layers is less than 1×10^{17}, the power of the second harmonic signal remains basically unchanged. As the doping concentration of cliff layers further increases, the power of the second harmonic signal decreases. Due to the role of the cliff layer, the electric intensity at the heterojunction increases, and the electric field extends towards the absorption region, reducing the transit time and accumulation degree of electrons in the absorption region, thereby suppressing the space charge effect. The doping concentration of the cliff layer at around 1×10^{18} can fully suppress the space charge effect, so the second harmonic power also reaches its minimum value when the cliff layer can play its maximum role. For the case of low input optical power, a large second harmonic signal power can be generated when there is no cliff layer or the doping concentration of the cliff layer is less than 1×10^{17}. In order to simplify the layer structure of the photodetector, the case of no cliff layer can be selected as the device structure for low input optical power.

The changes in fundamental and second harmonic power of the initial structural device (The doping concentration

of the cliff layer is 1×10^{18}) under different collection layer thicknesses are shown in Fig. 7. As the collection layer thickness increases, both fundamental and second harmonic power show a certain degree of increase. For UTC-PD, photo generated electrons mainly drift in the collection layer. The increase in the thickness of the collection layer reduces the electric intensity of the collection layer, making it easier for photo generated electrons to accumulating, enhancing the space charge effect, and increasing the frequency doubling output power. Under low input light power conditions, this article selects a 500 nm collection layer to obtain a larger frequency doubling output power.

The change in the thickness of the absorption layer of the photodetector will significantly affect the RF output power of the device. On the basis of the optimization results in the previous text (No cliff layer, collection layer thickness of 500 nm), Fig. 8 shows the variation of the fundamental and second harmonic power of the photodetector with the thickness of the absorption layer. The second harmonic power shows a trend of first increasing and then decreasing with the increase of the absorption layer thickness. As the increase of the absorption layer thickness directly leads to an increase in responsiveness, more photo generated carriers can be generated under the same input optical power conditions, which increases the space charge effect inside the device, The output power of nonlinear signals increases. When the thickness of the absorption layer is larger than 300 nm, the device has reached saturation state. Therefore, as the thickness of the absorption layer further increases, the second harmonic output power shows a decreasing trend.

The optimized structure of the photodetector based on the above results is shown in Table 2. The second harmonic signal power of the device was simulated under different incident optical powers, and the comparison with the initial structure of the photodetector is shown in Fig. 9. Compared with the initial structure of the device, the saturated optical power of the new structure is reduced, and the peak output of the second harmonic is correspondingly reduced. However, under low incident optical power, the second harmonic output power of the device is significantly improved. At an input optical power of 5×10^3 W/cm^2, the second harmonic output power increases from -55dBm to -30dBm.

4.2 High input optical power situation

This section analyzes the second harmonic signal power of photodetectors under large or unrestricted input optical power conditions. Under other unchanged conditions, an input optical power of 4×10^4 W/cm^2 is selected to study the effects of cliff layer doping concentration, spatial layer doping concentration, and collection layer thickness changes on
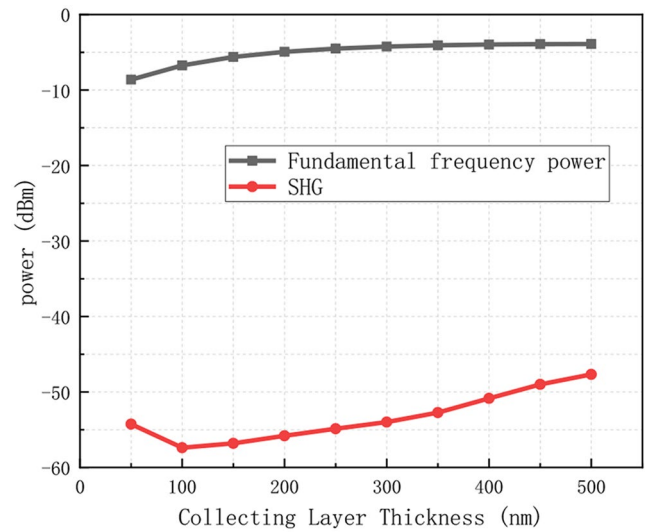
Fig. 7 The variation of fundamental and second harmonic power with the thickness of the collection layer (Low input optical power situation)
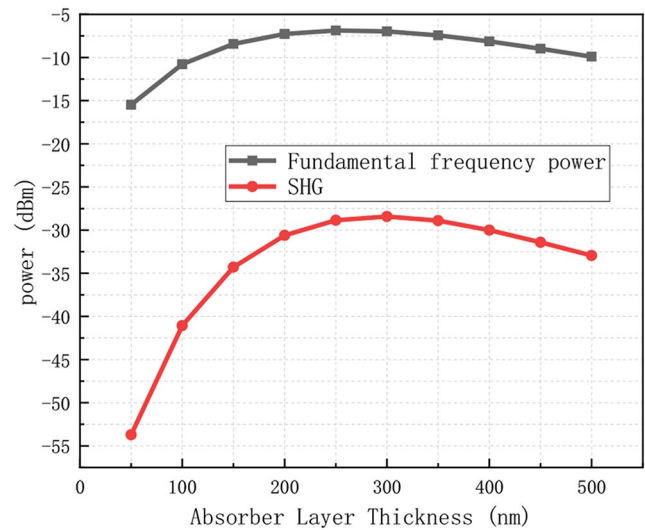
Fig. 8 The variation of fundamental and second harmonic power with the thickness of the absorption layer (Low input optical power situation)

Table 2 New epitaxial layer structure

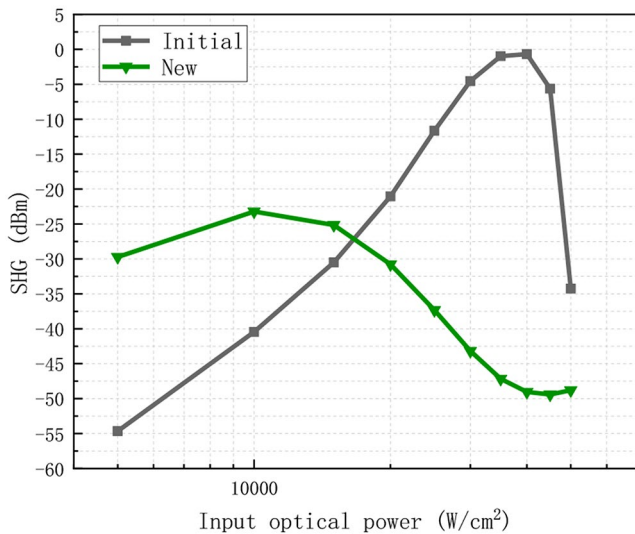| Layer	Material	Bandgap (eV)	Thickness (nm)	Dopant Type	Doping Level (cm^{-3})
P contact	InGaAs	0.73	50	P	3e19
Block	InGaAsP	1.105	20	P	2e19
P absorption	InGaAs	0.73	300	P	1e18
Gap grading	InGaAs	0.73	8	Undoped	1e15
Gap grading	InGaAsP	1.0	16	Undoped	1e15
Gap grading	InP	1.35	6	Undoped	1e15
Collection	InP	1.35	500	N	1e16
Sub Collection	InP	1.35	50	N	5e18
N contact	InP	1.35	500	N	1e19

Fig. 9 The variation of second harmonic power with input optical power before and after optimization design

the fundamental frequency output power and second harmonic signal power.

Figure 10 shows the results of RF output power under different doping concentrations of cliff layer and spatial layer. The initial doping concentration point (5×10^{14}) in the figure represents the device structure without cliff layer (no spatial layer). It can be observed that the fundamental frequency output power in the figure has undergone significant changes. This is because the optical power of the device itself is located near the saturation point, so slightly changing the device structure will lead to a change in the saturation state of the device. As shown in Fig. 10(a), the doping concentration of the cliff layer can only increase

the electric intensity at the heterojunction when it is around 1×10^{18}, and the electric field extends towards the absorption region, reducing the transit time and accumulation degree of electrons in the absorption region, thereby leading to an increase in saturation current. If the doping concentration of the cliff layer is too high or too low, it cannot achieve the corresponding effect of increasing saturation current, so the second harmonic power also reaches its maximum value when the cliff layer can play its maximum role. The corresponding Fig. 10(b) can also reflect the changes in the saturation state of the device. When there is no spatial layer or the doping concentration in the spatial layer is too high, it cannot smooth the conduction band and enable electrons to pass through the heterojunction better. Overall, changing the doping concentration in the cliff layer and spatial layer affects the space charge effect of the device and changes the original saturation point, thereby changing the RF output power.

The following figure (Fig. 11) shows the effect of changing the thickness of the collection layer of the photodetector on the RF output power of the device under high incident optical power. The nonlinear signal power of the photodetector shows a trend of first increasing and then decreasing with the increase of the collection layer thickness. Observing the curve of SHG in the figure, it can be observed that the variation pattern of second harmonic frequency before the thickness of the 300 nm collection layer is consistent with the result of lower optical power in the previous section. According to the research results in the previous section, corresponding to the initial structure of the 263 nm collection layer thickness, the optical power of 4×10^4 W/cm^2 is the saturation point of the initial structure device.
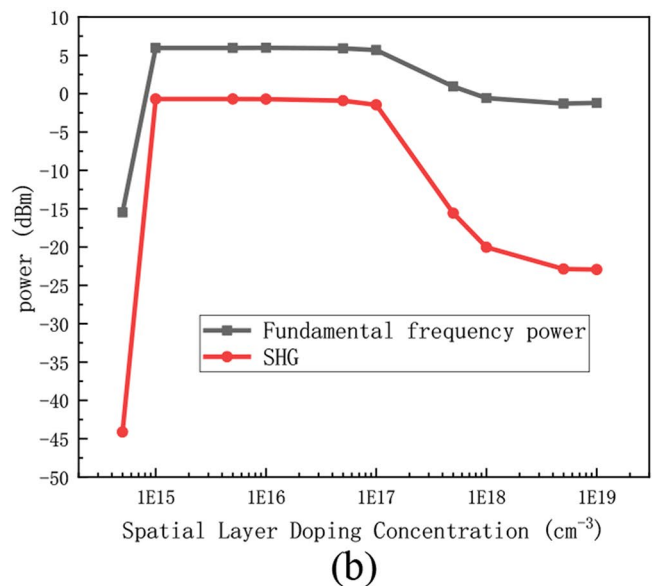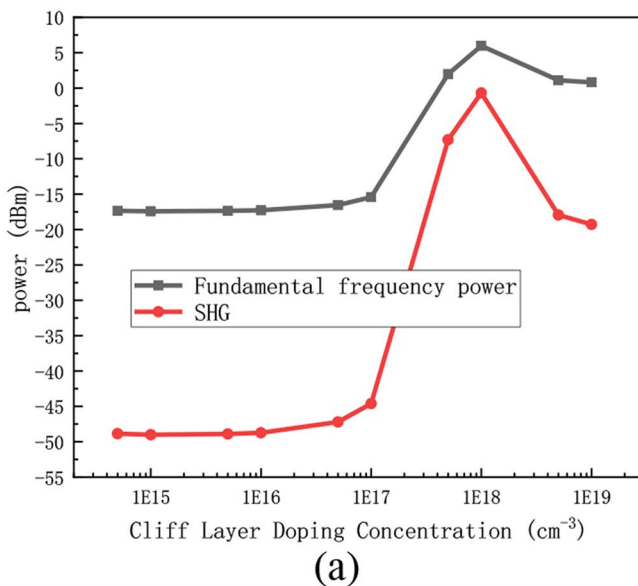

Fig. 10 The variation of fundamental and second harmonic power with doping concentration in the cliff layer (**a**) and spatial layer (**b**) (High input optical power situation)
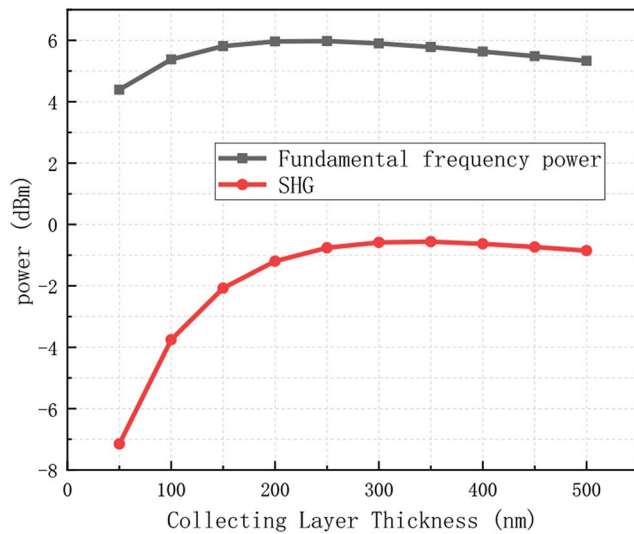
Fig. 11 The variation of fundamental and second harmonic power with the thickness of the collection layer (High input optical power situation)
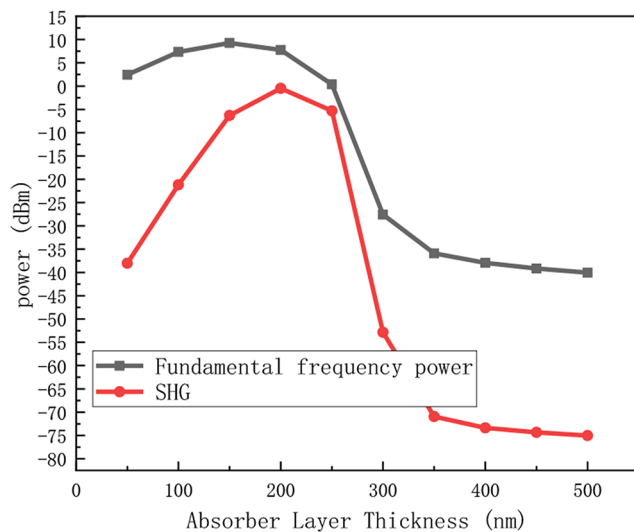

Fig. 12 The variation of fundamental and second harmonic power with the thickness of the absorption layer (High input optical power situation)

However, as the collection layer thickness increases, the internal electric intensity of the device gradually decreases, and the influence of space charge effect on the device will increase. This means that the saturated optical power of the device decreases with the increase of the collection layer thickness. The working state of the photodetector has not reached saturation before the collection layer thickness of 300 nm, which still belongs to the category of "small incident optical power" for the device itself. Therefore, as the collection layer thickness increases, the space charge effect of the device strengthens, leading to an increase in the frequency doubling signal; But when the thickness of

the collection layer further increases to above 300 nm, the device is already in a saturated working state. Further increase in the thickness of the collection layer will only enhance the space charge effect, which is not conducive to the second harmonic signal output of the photodetector, and the nonlinear signal power will decrease.

Figure 12 shows the variation of the fundamental frequency power and second harmonic power with the thickness of the absorption layer. Based on the conclusion from the previous section on the low input optical power situation, as the thickness of the absorption layer increases, the number of photo generated carriers increases, and the space charge effect becomes stronger. When the device does not reach saturation, the frequency doubling output power increases with the increase of the absorption layer thickness. After the device reaches saturation, the increase of the absorption layer thickness causes a rapid decrease in RF output power. When the absorption layer thickness is 220 nm, it can just make the current input optical power of the photodetector reach saturation.

It is not difficult to see from the results that the initial structure of the photodetector is already in the range of maximum output power. This is because the design of the photodetector with the initial structure was originally intended for high-power applications, and high-power photodetectors need to be able to effectively suppress the space charge effect to operate at higher incident optical power. This is consistent with the concept of designing photodetectors that generate high frequency doubling signals. Therefore, for the pursuit of peak frequency doubling power, the current high-power photodetector layer structure and design concepts can be applied.

4.3 Optimization of incident optical field distribution

Research has shown that by adjusting the distance between the incident fiber and the photodetector [19] or shaping the incident beam using a grating design [20], the concentration of incident optical power can be changed. The optical power of high frequency light is mainly concentrated at the center of the device, the central axis of the Gaussian beam coincides with the center of the device. The optical intensity distribution curve at the diameter of the device is shown in Fig. 13 (when the x-coordinate exceeds 5 μm, the optical power under Gaussian distribution has approached 0 W/cm^2, so the situation where the x-coordinate exceeds 5 μm is not shown in the figure). Set the center position coordinate of the device to x = 0 μm. The expression for the transverse optical field distribution of a Gaussian beam provided by Silvaco TCAD is
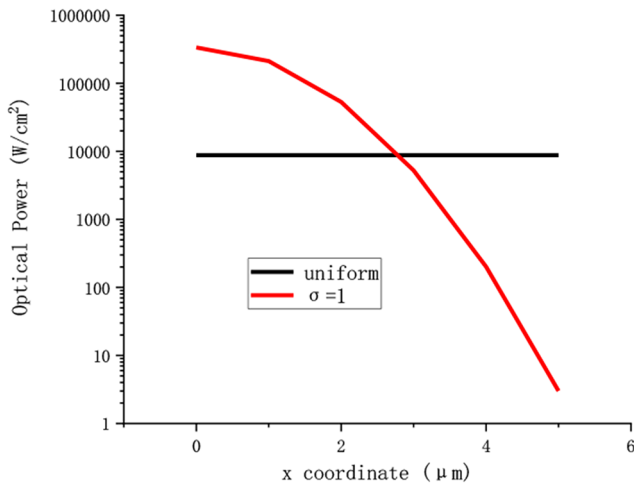
Fig. 13 Uniform optical field and σ = 1 Gaussian optical field distribution (0 coordinates represent the central axis position of the device)
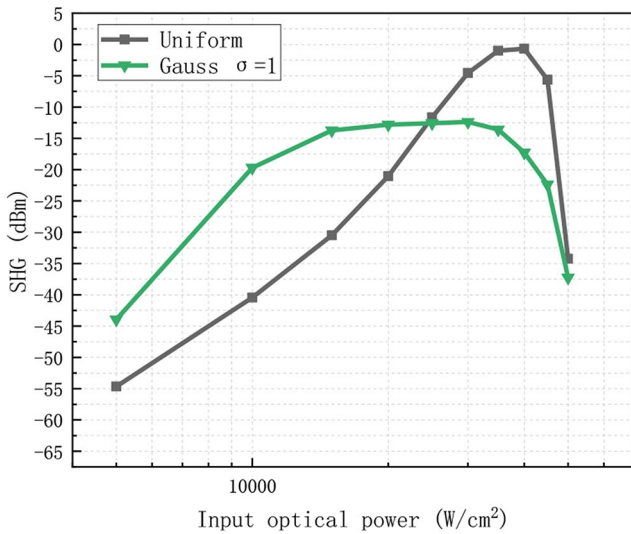

Fig. 14 The variation of second harmonic power with input optical power under uniform and Gaussian optical field distributions

$$f\left(x\right) = \frac{1}{\sigma\sqrt{2\pi}}\exp\left(-\frac{x^2}{2\sigma^2}\right) \qquad (2)$$

X is the distance between a point in the beam and the central axis. Definition σ as the waist width of a Gaussian beam can characterize the degree of concentration of incident optical power. The incident optical power in the active region of the device is

$$P = \int_0^r 2\pi\,x\cdot f\left(x\right)dx \qquad (3)$$

Where r is the active region radius of the device. In this study, the active region radius of the device was 10 μm.

When the optical power of uniform beam is 1 W/cm^2, under the same optical power, the waist width of the beam σ = 1 The Gaussian peak optical power density of is 40 W/cm^2.

The change in the distribution of incident optical field will change the distribution of photo generated carriers inside the device, thereby affecting the space charge effect of the photodetector, resulting in a change in the frequency doubling output of the photodetector. Figure 14 compares the frequency doubling output power of uniform optical with Gaussian beam with σ = 1 for the same power. The conclusion is that under low incident optical power, Gaussian optical field conditions have higher nonlinear power. This is because the photogenerated carriers generated by Gaussian beam are mainly concentrated at the central axis position of the device, and the carrier concentration in the central part is significantly higher. Therefore, the space charge effect of the device will be more obvious, and the frequency doubling output power of the photodetector will also be higher. Under high incident optical power conditions, uniform light field distribution results in higher nonlinear power, which is opposite to low input optical power. The reason for this is that under uniform optical field conditions, the distribution of photo generated carriers is more uniform, and the space charge effect saturates the device only when the optical power is high. Therefore, under high input optical power, uniform beam can achieve greater peak frequency doubling power.

5 Conclusion

In this article we investigate the mechanism of nonlinear signal generation in photodetectors and utilizes the nonlinear frequency doubling effect to generate millimeter wave signals. On this basis, the structure of the photodetector is further optimized and designed. For low incident optical power situations, the optimized structure of the photodetector increases the frequency doubling output power by 25dB on the basis of the original structure; For high input optical power, when the reverse bias is 1 V and the input power is 4×10^4W/cm^2 the output power of the second harmonic signal of the device can reach 0dBm, and research shows that high saturation devices have a decisive effect on the peak frequency doubling output power. Finally, the influence of optical field distribution on the nonlinear output power of photodetectors was analyzed. Under Gaussian optical field distribution, a more concentrated input optical power can improve the frequency doubling output of the device at low optical power.

Data availability No datasets were generated or analysed during the current study.

Declarations

Ethical approval Not applicable.

Competing interests The authors declare no competing interests.

References

1. J. Yao, Microwave photonics. J. Lightwave Technol. **27**, 314–335 (2009)
2. L. Goldberg, H. Taylor, J. Weller, D. Bloom, Microwave signal generation with injection-locked laser diodes. Electron. Lett. **13**, 491–493 (1983)
3. J. Harrison, A. Mooradian, Linewidth and offset frequency locking of external cavity GaAlAs lasers. IEE J. Quantum Electron. **25**, 1152–1155 (1989)
4. R. Ramos, A. Seeds, Fast heterodyne optical phase-lock loop using double quantum well laser diodes. Electron. Lett. **1**, 82–83 (1992)
5. U. Gliese et al., A wideband heterodyne optical phase-locked loop for generation of 3–18 GHz microwave carriers. IEEE Photonics Technol. Lett. **4**, 936–938 (1992)
6. A. Bordonalli, C. Walton, A.J. Seeds, High-performance phase locking of wide linewidth semiconductor lasers by combined use of optical injection locking and optical phase-lock loop. J. Lightwave Technol. **17**, 328 (1999)
7. K. Williams, L. Goldberg, R. Esman, M. Dagenais, J. Weller, GHz offset phase-locking of nd: YAG 1319 nm nonplanar ring lasers. Electron. Lett. **18**, 6–34 (1989)
8. F. Fan, M. Dagenais, Optical generation of a megahertz-linewidth microwave signal using semiconductor lasers and a discriminator-aided phase-locked loop. IEEE Trans. Microwave Theory Tech. **45**, 1296–1300 (1997)
9. H.R. Rideout, J.S. Seregelyi, S. Paquet, J. Yao, Discriminator-aided optical phase-lock loop incorporating a frequency down-conversion module. IEEE Photonics Technol. Lett. **18**, 2344–2346 (2006)
10. J. O'reilly, P. Lane, R. Heidemann, R. Hofstetter, Optical generation of very narrow linewidth millimetre wave signals. Electron. Lett. **25**, 2309–2311 (1992)
11. J. O'Reilly, P. Lane, Remote delivery of video services using mm-waves and optics. J. Lightwave Technol. **12**, 369–375 (1994)
12. J. O'reilly, P. Lane, Fibre-supported optical generation and delivery of 60 GHz signals. Electron. Lett. **30**, 1329–1330 (1994)
13. P. Shen et al., in MWP 2003 Proceedings. International Topical Meeting on Microwave Photonics, 2003. 189–192 (IEEE)
14. X. Chen, Z. Deng, J. Yao, Photonic generation of microwave signal using a dual-wavelength single-longitudinal-mode fiber ring laser. IEEE Trans. Microwave Theory Tech. **54**, 804–809 (2006)
15. K.J. Williams, R.D. Esman, M. Dagenais, Nonlinearities in pin microwave photodetectors. J. Lightwave Technol. **14**, 84–96 (1996)
16. T. Ishibashi, H. Fushimi, H. Ito, T. Furuta, in International Topical Meeting on Microwave Photonics. MWP'99. Technical Digest. (Cat No **99EX301**). 75–78 (IEEE).
17. G. Ghione, *Semiconductor Devices for high-speed Optoelectronics*, vol. 116 (Cambridge University Press Cambridge, 2009)
18. T. Umezawa et al., Bias-free operational UTC-PD above 110 GHz and its application to high baud rate fixed-fiber communication and W-band photonic wireless communication. J. Lightwave Technol. **34**, 3138–3147 (2016)
19. A. Beling, H. Pan, H. Chen, J.C. Campbell, in 2008 IEEE MTT-S International Microwave Symposium Digest. 499–502 (IEEE)
20. C. Xie et al., in Asia Communications and Photonics Conference. M4A. 136 (Optica Publishing Group)